APL Materials

RESEARCH ARTICLE | AUGUST 30 2024

Utilizing $(Al, Ga)_2O_3/Ga_2O_3$ superlattices to measure cation vacancy diffusion and vacancy-concentration-dependent diffusion of Al, Sn, and Fe in β-Ga_2O_3

Nathan D. Rock ; Haobo Yang ; Brian Eisner ; Aviva Levin ; Arkka Bhattacharyya ; Sriram Krishnamoorthy ; Praneeth Ranga ; Michael A. Walker; Larry Wang ; Ming Kit Cheng ; Wei Zhao; Michael A. Scarpulla

APL Mater. 12, 081101 (2024)
https://doi.org/10.1063/5.0206398

Utilizing $(Al, Ga)_2O_3/Ga_2O_3$ superlattices to measure cation vacancy diffusion and vacancy-concentration-dependent diffusion of Al, Sn, and Fe in $\beta - Ga_2O_3$

Cite as: APL Mater. 12, 081101 (2024); doi: 10.1063/5.0206398
Submitted: 1 March 2024 • Accepted: 4 July 2024 •
Published Online: 30 August 2024

Nathan D. Rock,[1] Haobo Yang,[1] Brian Eisner,[1] Aviva Levin,[1] Arkka Bhattacharyya,[2,3] Sriram Krishnamoorthy,[2,3] Praneeth Ranga,[2] Michael A. Walker,[4] Larry Wang,[5] Ming Kit Cheng,[5] Wei Zhao,[5] and Michael A. Scarpulla[1,2,a)]

AFFILIATIONS

[1] Department of Materials Science and Engineering, University of Utah, Salt Lake City, Utah 84112, USA
[2] Department of Electrical and Computer Engineering, University of Utah, Salt Lake City, Utah 84112, USA
[3] Materials Department, University of California, Santa Barbara, Santa Barbara, California 93106, USA
[4] Department of Metallurgical and Materials Engineering, Colorado School of Mines, Golden, Colorado 80401, USA
[5] Eurofins EAG Material Science, Sunnyvale, California 94086,

[a)] Author to whom correspondence should be addressed: mike.scarpulla@utah.edu

ABSTRACT

Diffusion of native defects such as vacancies and their interactions with impurities are fundamental to semiconductor crystal growth, device processing, and design. However, the transient equilibration of native defects is difficult to directly measure. We used $(Al_xGa_{1-x})_2O_3/Ga_2O_3$ superlattices (SLs) to detect and analyze transient diffusion of cation vacancies during annealing in O_2 at 1000–1100 °C. Using a novel finite difference scheme for diffusion with time- and space-varying diffusion constants, we determined diffusion constants for Al, Fe, and cation vacancies, including the vacancy concentration dependence for Al. In the case of SLs grown on Sn-doped $\beta - Ga_2O_3$ (010) substrates, gradients observed in the extent of Al diffusion indicate a supersaturation of vacancies in the substrates that transiently diffuse through the SLs coupled strongly to Sn and thus slowed compared to undoped cases. In the case of SLs grown on (010) Fe-doped substrates, the Al diffusion is uniform through the SLs, indicating a depth-uniform concentration of vacancies. We find no evidence for the introduction of V_{Ga} from the free surface at rates sufficient to affect Al diffusion at at. % concentrations, establishing an upper bound on surface injection. In addition, we show that unintentional impurities in Sn-doped Ga_2O_3 such as Fe, Ni, Mn, Cu, and Li also diffuse toward the surface and accumulate. Many of these likely have fast interstitial diffusion modes capable of destabilizing devices, thus suggesting that impurities may require further reduction. This work provides a method to measure transients in diffusion-mediating native defects otherwise hidden in common processes such as ion implantation, etching, and film growth.

I. INTRODUCTION

$\beta - Ga_2O_3$ is an ultra-wide bandgap (UWBG) semiconductor with potential for a superior performance in power electronics as well as in solar blind UV photodetectors and in transparent contacts for photovoltaics.[1–3] To further advance this technology, a thorough understanding of native and impurity defect processes during, for example, single crystal growth, epitaxial growth, and other fabrication steps must be developed.

Many groups have observed the formation of insulating surface layers on *n*-type $\beta - Ga_2O_3$ during annealing in air or O_2.[4–6] This formation of an insulating surface layer allows for facile formation of UV photodetectors. This phenomenon was originally attributed to the elimination of V_O, which were presumed to act as shallow donors, before refined DFT calculations indicated that V_O was a deep donor unable to contribute directly to *n*-type conductivity.[7] Oshima *et al.* documented the $\sqrt{t}$ kinetics of the insulating layer

thickness formed during O_2 annealing and demonstrated that an SiO_2 cap could prevent it.[5] This indicates that direct exposure of the Ga_2O_3 surface to oxygen does control the compensation of *n*-type conductivity in some way. Meanwhile, positron annihilation experiments have demonstrated the presence of V_{Ga} in both bulk crystals and thin films.[8,9] These experiments show increases in V_{Ga} concentration or charge states accompany O_2 annealing, which makes them a strong candidate for *n*-type compensation.[10,11] Many mechanisms, involving oxygen, V_{Ga}, V_O, and *n*-type dopants (Sn and Si), have been proposed. Some of these involve defect complexes instead of bare V_{Ga} and V_O.[12–15] Despite these existing studies, the specific mechanisms and rates of V_{Ga} introduction via processes such as bulk defect pair formation, climb of dislocations, injection from other structural defects, or in-diffusion from surfaces remain unknown. At the root, this is because native defects such as vacancies and interstitials are significantly more difficult to observe than, for example, impurity atoms.

With the exception of the direct interstitial impurity mechanism, self- and tracer-diffusion is mediated by native defects such as vacancies or interstitials.[3,16–22] Low concentrations of isovalent substitutional cations in oxides should exhibit primarily vacancy-mediated mechanisms under oxygen-rich conditions, provided that the radius of the cation is not significantly less than that of the host atom. Such conditions will favor cation vacancies and suppress cation interstitials. Interstitial mediated mechanisms may be possible under metal-rich conditions, which favor cation interstitials. The diffusion constant of isotopic or chemical tracers is proportional to the local concentration of mediating native defects and the correlation factor parameterizing their interactions such as complexation. Thus, for vacancy mediated hopping, the tracer diffusion "constant" can vary in space and time with the concentration of mediating vacancies. Different samples may exhibit different diffusion constants by virtue of their vacancy content, an effect that may explain the typical scatter of experimental diffusion rates. This, in turn, can be affected by dopant impurities through Fermi level effects as well as the samples' thermal and chemical history. For dopant ions that control the local Fermi level, the local equilibrium of native defects can result in that dopant's diffusion constant being dependent on its own concentration.[23–29]

Commonly, it is assumed (and in careful experiments, ensured) that diffusion-mediating native defects rapidly equilibrate with local impurity concentrations compared to the experimental timescale. Rapid equilibration can be assumed in samples containing dense sources and sinks such as polycrystals; however, in high-perfection crystals like those in this study, equilibration may be limited by injection at or transport from remote surfaces. Experiments in which native defect processes occur on similar timescales to tracer or impurity diffusion translate to time- and space-varying vacancy concentrations and thus time- and space-varying impurity diffusion constants. A technologically important example is ion implantation in which massive supersaturations of native defects are created in distributions spatially correlated with the implanted impurity profile, which provides an alternative mechanism of concentration-dependent diffusion for short timescales and low temperatures[30,31] applicable to both dopants and isovalent impurities. Etching and layer deposition may also inject native defects from the free surface.[32]

Herein, we grow and isothermally anneal superlattices (SLs) consisting of isovalent Al tracer concentration spikes in β-Ga_2O_3. We use these SLs to investigate the diffusion of cation vacancies (V_{Ga}), the interdiffusion of Al, and the diffusion of intentional dopants (Fe or Sn). Al diffusion in superlattices epitaxially grown on Fe substrates occurs with spatially uniform vacancy density, while in samples grown on Sn-doped wafers, we show strong evidence for transient diffusion of cation vacancies out of the substrate. Using a novel modification of the Crank–Nicolson finite difference scheme, we infer the diffusion of the vacancies mediating Al diffusion. The final Al profiles in this work record a weighted time average of $[V_{Ga}]$ at each depth. The $D_{V_{Ga}}$ we extract should also be understood as a time-averaged value in the presence of certain Sn (donor) or Fe (acceptor) concentrations and small amounts of Al. Our experiments thus set lower bounds on the true $D_{V_{Ga}}$ and Ga self-diffusion constant for single crystalline $\beta - Ga_2O_3$. We determine the diffusion constants for Al including its dependence on local V_{Ga} concentration, for V_{Ga} (likely in the form of Sn_{Ga}–V_{Ga} complexes), and for Fe under conditions of low vacancy concentration and low electron density. Finally, we serendipitously discovered that many other cation species such as Fe, Mn, Ni, Li, and Cu also diffused from the EFG-grown Sn-doped substrates and accumulated near the free surface.

II. EXPERIMENTAL AND NUMERICAL METHODS

Superlattices (SLs) consisting of 6 or 9 alternating layers of 200 nm unintentionally doped (UID) $\beta - Ga_2O_3$ and 10–15 nm $(Al_xGa_{(1-x)})_2O_3$ (AlGO), where $x \cong 0.05$ were epitaxially grown using organometallic vapor phase epitaxy (OMVPE) in an Agnitron Agilis 100 system on (010) Sn or Fe doped $\beta - Ga_2O_3$ substrates obtained from Novel Crystal Technology (NCT) grown by edge fed growth (EFG). The vendor reports Fe or Sn concentrations in the mid-10^{18} cm^{-3}, and etch pits from nanovoids and dislocations are $<10^5/cm^2$. The lowest practical Al concentration of ≈5 at. % was used, and layers below the critical thickness were used in order to prevent introduction of misfit dislocations. SLs always began and ended with 200 nm Ga_2O_3 spacers. UID layers grown under the same conditions exhibit *n*-type doping in the low $10^{16}/cm^3$ range. Annealing was carried out for times between 2 and 80 h with the SL side of the sample exposed to O_2 in a quartz tube furnace in 1 atm of flowing O_2. Prior to annealing, the annealing tube and the quartz or sapphire plates on which samples sat were etched with aqua regia to remove any metal contamination. During annealing, temperature was ramped at 10 °C/min and then held constant for the indicated time, after which it was allowed to freely return to room temperature.

Dynamic secondary ion mass spectroscopy (d-SIMS) profiles were collected before and after annealing on each individual sample by EAG Eurofins. The depth was calibrated by measured crater depths and concentrations using ion implanted composition standards. Comparing multiple SIMS profiles from each sample and between samples as well as x-ray diffraction Pendellösung fringes allowed us to quantify the uncertainty in depth scales, resulting primarily from growth rate variation, of at most $\Delta x = \pm 6\%$. This translates to relative uncertainty in extracted diffusion constants of order $(\Delta x)^2 = \pm 0.4\%$, which we expect is much smaller than uncertainties from sample to sample variations in doping and defects. The

annealing temperature accuracy at the location of the samples was measured to be within a few degrees of nominal.

The most general microscopic formulation of tracer diffusion problems is coupled reaction–diffusion of defects and complexes wherein the tracer-native defect complexes have different diffusion coefficients than the isolated species.[33,34] The fraction of time, or population fraction, of complexes relates to the binding energy and connects to the correlation coefficient of random walk theory.[20]

Vacancy mediated diffusion of Al is assumed due to the chemical similarity of Ga and Al. Somewhat surprisingly, numerical treatment in the case of non-steady-state vacancy-mediated diffusion is not widely considered. Thus, a novel numerical approach based on the Crank–Nicolson scheme (second-order centered finite differences in space, forward and linear in time) was developed. We assume the local Al diffusion constant, D_{Al}, to be Arrhenius activated and proportional to the local concentration of cation vacancies (shorthanded as $[V_{\mathrm{Ga}}]$ in number/cm^3 acknowledging the small Al content). It thus takes the following form:

$$D_{\mathrm{Al}} = D_o \cdot \exp\left(\frac{-E_a}{k_B T}\right) = D^* \cdot [V_{\mathrm{Ga}}] \cdot \exp\left(\frac{-E_a}{k_B T}\right) = D_{oo}(T) \cdot [V_{\mathrm{Ga}}], \tag{1}$$

in which D_o (cm^2/s) is the conventional prefactor, D^* (cm^5/s) is a constant for all temperatures, E_a is the Al hopping activation energy given a neighboring vacancy, k_B is Boltzmann's constant, T is absolute temperature, and $D_{oo}(T) = D^* \exp\left(\frac{-E_a}{k_B T}\right)$ is a constant at each temperature. Fick's second law for isothermal tracer Al diffusion becomes

$$\begin{aligned}\frac{\partial[\mathrm{Al}]}{\partial t} &= \frac{\partial}{\partial x}\left(D_{\mathrm{Al}}\frac{\partial[\mathrm{Al}]}{\partial x}\right) = \frac{\partial D_{\mathrm{Al}}}{\partial x}\frac{\partial[\mathrm{Al}]}{\partial x} + D_{\mathrm{Al}}\frac{\partial^2[\mathrm{Al}]}{\partial x^2} \\ &= D_{oo}\left\{\frac{\partial[V_{\mathrm{Ga}}]}{\partial x}\frac{\partial[\mathrm{Al}]}{\partial x} + [V_{\mathrm{Ga}}]\frac{\partial^2[\mathrm{Al}]}{\partial x^2}\right\}.\end{aligned} \tag{2}$$

Not assuming spatial uniformity of the diffusion constant introduces the cross-derivative term involving gradients of both [Al] and $[V_{\mathrm{Ga}}]$.

The second-order space central difference, first-order forward time discretization of this equation on a uniform grid of spacing Δx is

$$\begin{aligned}\frac{u_N^{j+1} - u_N^j}{\Delta t} = \frac{1}{8\Delta x^2}\Big[&u_{N-1}^j(D_{N-1}^j + 4D_N^j - D_{N+1}^j) + u_{N-1}^{j+1} \\ &\times (D_{N-1}^{j+1} + 4D_N^{j+1} - D_{N+1}^{j+1}) - 8(u_N^j D_N^j + u_N^{j+1} D_N^{j+1}) \\ &+ u_{N+1}^j(-D_{N-1}^j + 4D_N^j + D_{N+1}^j) \\ &+ u_{N+1}^{j+1}(-D_{N-1}^{j+1} + 4D_N^{j+1} + D_{N+1}^{j+1})\Big],\end{aligned} \tag{3}$$

in which the space and time grids are indexed, respectively, by the superscript j and subscript N and Δx and Δt are the x and t intervals, respectively. Dirichlet and von Neumann boundary conditions were applied for Al at the deepest points in the substrate and surface, respectively. To simplify simulation, which we implemented in MATLAB,[35] we used analytical solutions for the diffusion of $[V_{\mathrm{Ga}}]$, which is tantamount to assuming that vacancy diffusion does not depend on Al concentration. This assumption was justified by the chemical similarity of Al and Ga and the small maximum Al concentration. We find the best balance of assumptions and distinguishable differences in modeled profiles by assuming depth-constant (but distinct) initial $[V_{\mathrm{Ga}}]$ conditions in the OMVPE-grown SL layers and the EFG-grown substrates. Because of the high dynamic range of the SIMS data with low uncertainty (meaning that both the peaks and valleys of the Al profiles are measured with good signal-to-noise ratios), we chose to use the square difference of $\log_{10}([\mathrm{Al}])$ between the measured and simulated profiles (summed over the J points in each profile) as our goodness of fit (GOF) parameter,

$$GOF = \frac{1}{J-3}\sum_{j=0}^{J}\left(\log_{10}[\mathrm{Al}_{model}(j)] - \log_{10}[\mathrm{Al}_{SIMS}(j)]\right)^2. \tag{4}$$

$D_{V_{\mathrm{Ga}}}$, the product $[V_{\mathrm{Ga}}]_{subs} \cdot Doo$, and the ratio $[V_{\mathrm{Ga}}]_{epilayer}/[V_{\mathrm{Ga}}]_{subs}$ are the three free parameters (degrees of freedom) of each scenario directly extractable from the simulation/fitting and robustly determined for each annealed sample.

Rather narrow ranges of parameter values reproduce the Al profiles especially for the samples grown on Sn substrates. If we assume a value for $[V_{\mathrm{Ga}}]$ in the substrates (discussed below), minimizing the GOF across many diffusion simulations allows us to extract $[V_{\mathrm{Ga}}]$ in the epilayer, D_{oo} for the Al at each T_{anneal}, and $D_{V\mathrm{Ga}}$ at each T. Any difference between actual and assumed $[V_{\mathrm{Ga}}]_{subs}$ will affect $[V_{\mathrm{Ga}}]_{epilayer}$ and D_{oo}. Thus, if the actual concentration is later found to be 10× higher than assumed in our analysis, then D_{oo} would be 10× lower but $[V_{\mathrm{Ga}}]_{epilayer}$ also 10× higher. Uncertainties in the final extracted parameter values were estimated from the curvature of the GOF with respect to each parameter. Further discussion of numerical methods and error propagation are in the supplementary material.

III. EXPECTATIONS OF VACANCY INITIAL CONDITIONS AND INITIAL OBSERVATIONS ON AL DIFFUSION

First, we discuss expectations for the initial conditions of concentrations of V_{Ga} in the substrates and superlattices and then present and initially assess the SIMS data. An intuition for a completely ionic crystal suggests that V_{Ga} should exist only in the 3^- charge state and thus have concentration scaling $\propto \left(\frac{n}{n_i}\right)^3$ or $\propto \exp\left(\frac{-3E_f}{k_B T}\right)$.[36] Modern density functional theory (DFT) with hybrid functionals accurately predicts that defect charge states may change if E_f moves above or below charge transition levels and can account for complexation with other defects.[7,37] At equilibrium with all other factors held constant, the concentration of V_{Ga} should be proportional to the n-type doping concentration; however, differences in chemical potentials (e.g., p_{O_2}) and temperatures during bulk crystal and OMVPE growth will modify this ratio.

A number of experiments[8,9,11,13,38,39] have detected and studied cation vacancies; however, the most credible *quantification* of V_{Ga} or its complexes in Sn-doped wafers comes from the E_c-2.0 eV signal measured by deep level optical spectroscopy (DLOS). DLOS measurements on different but very similar OMVPE layers report a concentration of $\approx 10^{15}$/cm^3 for the E_c-2.0 eV defects,[40] while DLOS measurements of E_c-2.0 eV defects in NCT Sn-doped bulk crystals are reported at $0.8–1.2 \times 10^{16}$/cm^3 for wafers matching the nominal Sn concentration of those used herein ($[Sn] = 3.5–5 \times 10^{18}$/cm^3).[41] For analysis, we assume

$[V_{Ga}] = 10^{16}/cm^3$ vacancies in the Sn-doped substrates unless otherwise mentioned.

While it is possible that DLOS may not detect some vacancies bound in complexes, the near-unity doping efficiency measured for Sn in bulk substrates in the $10^{18}/cm^3$ range indicates that $[V_{Ga}]$ cannot be much larger. Unfortunately, junction capacitance based defect spectroscopies such as DLTS or DLOS cannot be performed on insulating samples, e.g., Fe-doped wafers or oxygen annealed ones; thus, comparable quantification is not available for Fe-doped substrates. All substrates were grown at T_{melt} ($k_B T_{melt} \approx 0.18$ eV) by EFG under reduced p_{O_2} conditions.[42,43] In Fe-doped Ga_2O_3, the Fermi level is pinned at the $Fe^{3+/2+}$ charge transition level corresponding to the 0/- transition of the Fe_{Ga} acceptor located very near E_c-0.8 eV by DLTS and related techniques.[44,45] Sn-doped substrates are degenerately doped or very close to it, thus $E_f \approx E_c$. For both of these E_f values, isolated V_{Ga} should be in the $q = 3^-$ charge state; thus, $[V_{Ga}^{3-}]$ in the Sn-doped substrates should be higher than in the Fe-doped substrates by a factor of $\exp\left(\frac{3\times 0.8\ eV}{0.18\ eV}\right) \approx 10^6$ if $[V_{Ga}]$ in both substrate types equilibrate at T_{melt}. If V_{Ga} stay equilibrated to a temperature lower than the freezing temperature, this ratio would increase, while if most of the V_{Ga} are in $(Sn_{Ga} - V_{Ga})^{2-}$ complexes or $(V_{Ga} - V_O)^-$ divacancy complexes, this ratio would be ~10^4 or 100, respectively. While the unintentional doping in our OMVPE layers grown at 800 °C is in the low 10^{16} /cm^3, it is very difficult to predict the ratio of $[V_{Ga}]$ in the SLs to those in the substrates because of the very different growth conditions. In addition, in unpublished experiments we have carried out, we find that annealing Sn-doped wafers in 1 atm O_2 at 1050 °C requires at least two weeks for full equilibration; thus, $[V_{Ga}]$ will not equilibrate in the full wafer during OMVPE growth. Thus, we consider the ratio of $[V_{Ga}]$ in the SL to that in the substrate to be an unknown parameter to be determined in the fitting. Despite the nominally identical growth of the superlattices, the initial conditions for the V_{Ga} or complexes mediating Al diffusion may be different from run to run, for those grown on Fe- or Sn-doped substrates, and from individual substrate to substrate.

Figures 1(a) and 1(b) show the Al and dopant SIMS profiles before and after annealing for 20 h in 1 atm O_2 at 1050 °C for two superlattices grown nominally identically on Sn- or Fe-doped substrates. For the SLs on Fe-doped substrates, Al diffuses without any detectable gradient in the extent of diffusion of the $(Al, Ga)_2O_3$ layers in the superlattices. Meanwhile, for SLs on Sn-doped substrates, the extent of Al diffusion is greater for $(Al, Ga)_2O_3$ layers closer to the substrate than the surface, and, overall, the Al diffusion is much faster. This is consistent with a larger $[V_{Ga}]$ in the Sn-doped substrates compared to the SLs and to that in the Fe-doped substrates, which diffuses through the SLs toward the surface on a non-negligible timescale compared to the annealing time. For both types of samples, we find no evidence for vacancy creation or in-diffusion from the free surface (e.g. greater extent of Al diffusion near the surface) at concentrations sufficient to affect Al diffusion from about 5 at. % down to $10^{18}/cm^3$. Such an effect could be taking place, but apparently at concentrations significantly lower than the estimated $10^{16}/cm^3$ from the Sn-doped substrates. In the case of Fe-doped substrates, V_{Ga} diffusion could be much faster than the time required for Al diffusion at the given V_{Ga} concentration such that it does equilibrate quickly compared to the experimental time. As discussed later, Sn_{Ga} donors form complexes with acceptor-like V_{Ga} but acceptor-like Fe_{Ga} do not; therefore, we should expect isolated V_{Ga} to diffuse faster through SLs grown on Fe-doped substrates. Figure 1(c) is a 3D rendering of a similar SL (this one having nine repeat units) constructed from Time of Flight (ToF)-SIMS after being annealed for 20 h at 1100 °C in O_2, showing the same behavior, with greater diffusion of Al near the SL/substrate interface.

IV. ANALYSIS OF Al AND Fe DIFFUSION FOR SLS ON Fe-DOPED SUBSTRATES

For SLs on Fe-doped substrates, uniform $[V_{Ga}]$ in the SL and substrate eliminates the cross-derivative term in Eq. (2) for the Al diffusion, reducing it to the usual form of Fick's second law. We tried many scenarios of different $[V_{Ga}]$ in the SL and substrate, but the best agreement with experiments was found for the case where both began with the same low concentration. Evolving the initial to final Al SIMS profiles for the sample annealed at 1050 °C allows us to

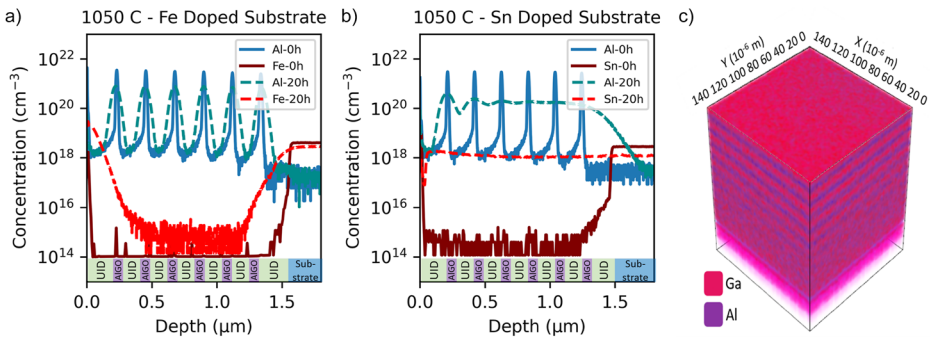

FIG. 1. Pre- and post-annealing quantified Al, Sn, and Fe SIMS profiles for superlattices grown on (a) Sn-doped and (b) Fe-doped substrates and annealed 20 h in 1 atm flowing O_2 at 1050 °C. The lower detection limits are $5 \times 10^{14}/cm^3$ for Fe, $5 \times 10^{15}/cm^3$ for Sn, and $3 \times 10^{17}/cm^3$ for Al. (c) 3D rendering of ToF SIMS data for a SL on the Sn-doped substrate after annealing at 1100 °C for 20 h, showing the lateral uniformity over an area 100 ×100 μm^2 and increasing intermixing deeper in the sample (compare to Fig. 2).

extract a value of $D_{Al} = D_{oo}(T) \cdot [V_{Ga}] = 3.5 \times 10^{-18}$ cm^2/s, assuming $[V_{Ga}] = 10^{14}$/cm^3, i.e., ≈100 times less V_{Ga} than for Sn-doped substrates, assuming $D_{oo}(T)$ is the same for both.

The diffusion of Fe itself appears to be complex, probably involving at least two modes such as interstitial and substitutional (which in turn may each involve different charge states). This conclusion is reached because, in addition to the [Fe] smoothly connected to that in the wafer, we established through many exacting experiments (see the supplementary material) that Fe additionally diffuses through the central portion of the SL and piles up near the surface—i.e., the [Fe] distribution near the surface is not a SIMS artifact nor does it arise from vapor phase transport. This accumulation at the surface was reproduced in both d- and ToF-SIMS, across multiple samples, and is also reproduced for Sn-doped substrates in which [Fe] is initially considerably lower in the substrate as discussed in Sec. VI. This requires a significantly faster diffusion mode such as interstitials and could also involve γ-Ga_2O_3.

The difference between the integrated Fe concentrations in the SL before and after annealing is ≈8.4×10^{13} cm^2. Of this, 8.0×10^{13}/cm^2 accumulated near the surface. The remaining 4×10^{12}/cm^2 Fe that diffused only short distances into the SL region apparently diffuses via a second, slower mode, which we presume to be substitutional hopping. Assuming that this corresponds to diffusion of Fe into a long half-space without complexation allows us to use the analytical solution to Fick's second law,[46]

$$C(x,t) = \frac{C_{subs} - C_{SL}}{2}\left(1 + erf\left[\frac{x - x_L}{\sqrt{Dt}}\right]\right), \quad (5)$$

in which C_{subs} and C_{SL} are the initial [Fe] concentrations in the substrate and SL, respectively, x_L is the depth of the SL/substrate interface, and D is the diffusion constant for Fe. Fitting the profile near the SL/substrate interface yields a diffusion constant of $D_{Fe} = 6 \times 10^{-16}$ cm^2/s. The diffusion of Fe and other transition metals in Ga_2O_3 certainly warrants additional experimental and theoretical scrutiny, including Fermi level effects. Fe is present at appreciable concentrations in most if not all Ga_2O_3 bulk crystals as an impurity introduced from raw materials or Ir crucibles and dies.[47]

V. ANALYSIS OF Al DIFFUSION FOR SLS ON Sn-DOPED SUBSTRATES

Figures 2(a)–2(c) present the initial and final SIMS profiles for [Al] for samples annealed at 1000, 1050, and 1100 °C for 20 h. The extent of Al diffusion within each SL is greater near the substrate than near the surface, indicating that the local concentration of $[V_{Ga}]$ was non-uniform and greater near the substrate for a significant portion of the annealing time. Samples (a) and (b) were grown in the same OMVPE growth run, while sample (c) was grown in a different run; this is important for understanding the smaller degree of Al diffusion despite this sample's higher annealing temperature, as discussed in more detail below. Figures 2(d) and 2(e) reproduce the data from (a) but also overlay simulated Al concentration profiles at 2 h intervals (red solid) for the best-fit parameters within two assumptions for V_{Ga} diffusion (green dashed) described in the following.

Diffusion parameter estimation from each experiment was accomplished by evolving the measured initial Al SIMS profile forward in time under many scenarios and fitting to the final SIMS profiles. Each tested scenario is defined by Eqs. (1) and (2), assuming initial $[V_{Ga}]$ in the SL and substrate, $[V_{Ga}]$ diffusion behavior explained below, and values for D_{oo} for Al and $D_{V_{Ga}}$. It is clear for all Sn-doped samples that the initial $[V_{Ga}]$ in the SLs must be at least 10 times lower than in the substrates, which agrees with intuition given the higher substrate n-type doping. The effects of $D_{V_{Ga}}$ and the initial $[V_{Ga}]$ ratio on the broadening and peak-to-valley [Al] ratio for each Al-containing layer in the SLs are sufficiently distinct that we can determine their values with low uncertainty within each scenario.

As shown in Fig. 2(d), we first tested the hypotheses that V_{Ga} diffuse freely without interactions from the Sn-doped substrate through the SLs according to the error function solution of Eq. (5).[46] These simulations were able to reproduce the final Al SIMS data extremely well as judged by inspection and by GoF values ≪1 as seen in Table I. Thus, the gradient in the extent of Al diffusion in the SLs on Sn-doped substrates is consistent with this hypothesized mechanism of out-diffusion of V_{Ga} from the substrate.

Since the [Al] depth profiles are essentially records of the time-integrated $[V_{Ga}]$ profile, it may not be possible to infer its exact functional shape from small numbers of experiments. However, the [Al] data very clearly show evidence for larger time integrated $[V_{Ga}]$ near the substrate, ruling out scenarios in which, for example, $[V_{Ga}]$ are introduced at the free surface and diffuse inward. In addition, it could be hypothesized that V_{Ga} are introduced under oxidizing conditions via Frenkel pair generation and out-diffusion of Ga_i. Since this mechanism creates electrically neutral pairs, it should occur at the same rate in the SLs, Fe-doped substrates, and Sn-doped substrates. Thus, any diffusion of Al enhanced by this mechanism would be depth-uniform and have an upper bound set by the rate observed in SLs on Fe-doped substrates—at least 2 orders of magnitude slower than for Sn-doped substrates. While this mechanism cannot be ruled out, it certainly cannot explain the experiments on Sn-doped substrates.

Diffusion of V_{Ga} according to Eq. (5) would imply that (a) the total number of V_{Ga} is conserved and (b) the *functional shape* of their concentration profile is unaffected by non-uniformities in [Sn](x, t) or [Al](x, t) (although the value of D_{VGa} may be affected). Since Al and Ga are chemically very similar, this is reasonable for Al. Frodason *et al.*[24] studied the diffusion of Sn from (001) Sn-doped substrates into UID HVPE-grown Ga_2O_3 at annealing temperatures 1050–1250 °C and fit them with a numerical reaction–diffusion (R–D) model. In their work (and in some similar intermediate Sn d-SIMS profiles obtained in this work but not shown herein), Sn diffuses with a front shape appearing on a log plot as a rounded step function. Sn is most stable as a substitutional Sn_{Ga} donor, and, thus, it is logical to expect that Coulomb attraction results in larger correlation for Sn than Al with V_{Ga}. Theoretical and experimental work has established fairly conclusively that Sn and V_{Ga} interact strongly while diffusing.[24,38,48]

During out-diffusion from Sn-doped substrates, V_{Ga} dynamically complex with (on average) a small fraction of the available Sn (since $[V_{Ga}] \ll [Sn_{Ga}]$). Complexed V_{Ga} diffuse slower than free V_{Ga}, while substitutional Sn_{Ga} diffuse only while complexed or correlated with a vacancy.[20] Critically for assessing how this will affect Al diffusion, the Sn_{Ga}–V_{Ga} complexation reaction's equilib-

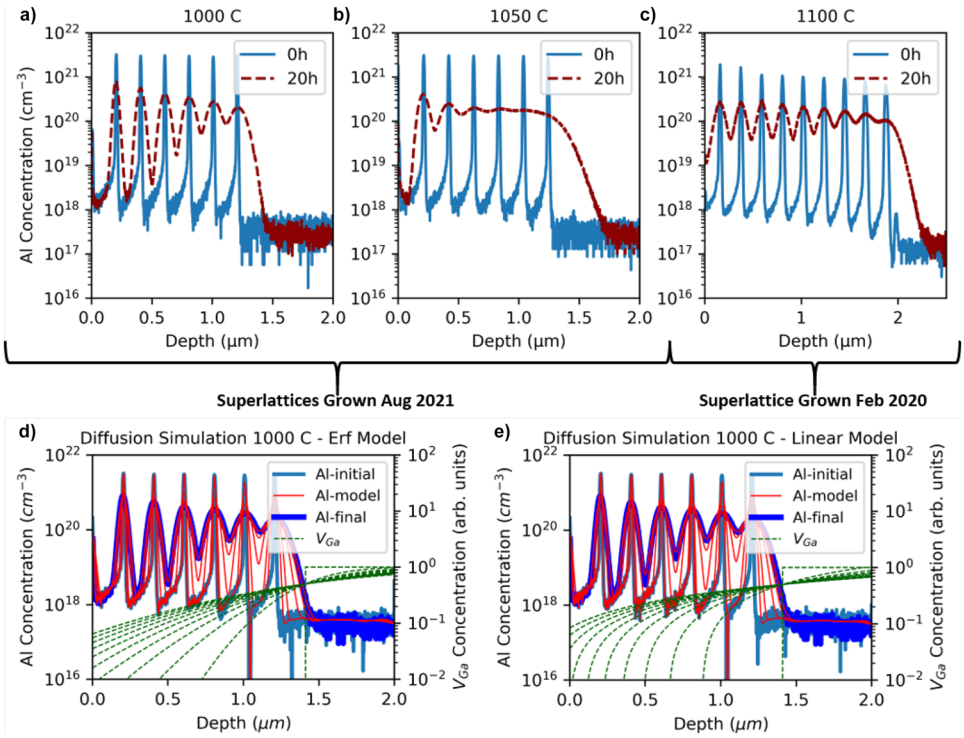

FIG. 2. (a)–(c) SIMS profiles of Al before (blue) and after (red) annealing for 20 h at the indicated temperatures. (d) and (e) Initial and final SIMS data from 1000 °C sample with the results of finite difference simulation shown in red for 2 h increments under the assumption that V_{Ga} diffuses as $erf(x,t)$ (d) or as piecewise linear solution to the Sn_{Ga}–V_{Ga} complex reaction–diffusion (e). Samples (a) and (b) were grown in the same OMVPE growth, while sample (c) was grown in a different run. The initial SIMS Al profiles were used as initial conditions for the finite difference code with space- and time-varying diffusion constants and evolved to the final time; computed profiles are shown in red for increments of 2 h. Goodness of fit values were computed for the final profiles sweeping a large range of the model parameter space in order to determine the best values of V_{Ga} initial step-function profiles, V_{Ga} diffusion constant, and proportionality constant between $[V_{Ga}]$ and D_{Al}. The assumed initial V_{Ga} step function profile is evolved using either the $erf(\,)$ assumption or the piecewise-linear approximation to the reaction diffusion of complexes, as shown in green dashed curves. The apparent decrease in the extent of Al diffusion between (b) grown at 1050 °C and (c) grown at 1100 °C is accounted for by a difference in the initial $[V_{Ga}]$ in the substrate, as explained in Sec. V.

rium rate constant was determined to be small in our temperature range, meaning that each complex is bound for only a short time before dissociating.[24] Therefore, V_{Ga} passing through the SLs has a high likelihood of assisting in Al diffusion even while co-diffusing with the Sn. The effective diffusion constant for V_{Ga} and thus for Ga and Al diffusion in the presence of donors such as Sn should be smaller than the value in intrinsic or acceptor-doped $\beta - Ga_2O_3$ (e.g., Fe-doped). The degree of retardation of cation vacancy diffusion will depend on the concentrations of donors and vacancies and thus be variable from experiment to experiment and vs depth and time within any diffusion experiment.

Since in our experiments, Sn also diffused through the SLs, our modeling should be at least consistent with these findings. Herein, it was not possible to implement a full numerical reaction–diffusion scheme involving V_{Ga}, Al, and Sn; while we did reproduce and test the numerical model used in Ref. 24, the unavailability of parameters for Al-containing defects and complexes meant that a simpler approach was needed. Thus, we developed an analytical approximation for the x and t evolution of both $[Sn_{Ga}]$ and $[V_{Ga}]$ within this R–D process during isothermal annealing (see the supplementary material). When plotted on a linear scale (which is relevant for the Al diffusion constant), the R–D front shapes are approximated well by a piecewise linear function defined as follows:

$$C(x,t) = \begin{cases} C_{subs} & C(x,t) > C_{subs}, \\ C_{epi} & C(x,t) < C_{epi}, \\ \dfrac{C_{\max}}{2}\left(1 + \dfrac{x - x_L}{\sqrt{Dt}}\right) & C_{epi} \geq C(x,t) \ldots \\ & \text{and } C(x,t) \geq C_{subs}. \end{cases} \quad (6)$$

At t = 0, this is a step function but the initially vertical section pivots vs time such that its intercepts with the max and min concentration values far away from the interface move as $\sqrt{Dt}$. This piecewise linear function accurately captures most of the dynamic range of the Sn_{Ga}–V_{Ga} steps from Ref. 24 and our re-analysis of those data. It only fails to capture the shape of the low-concentration leading edge of Sn diffusion (2–3 orders of magnitude below the minimum [Al] herein) and at high concentrations in the substrate (which is irrelevant for the SL diffusion). Since Al

TABLE I. Effective Al diffusion coefficient (D_{oo}) and gallium vacancy diffusion coefficient for the error function model and reaction–diffusion (R–D) linear model for SLs grown on Sn- and Fe-doped (010) $\beta - Ga_2O_3$ and annealed at 1000, 1050, and 1100 °C. In the Fe, a uniform initial V_{Ga} profile is assumed, so now the value for $D_{V_{Ga}}$ is reported. D_{oo} is given assuming indicated initial values for $[V_{Ga}]$ in the SL and substrate as explained in Sec. V.

Sample	Dopant	Diffusion model	Anneal temp (°C)	D_{oo} (cm^5/s)	$D_{V_{Ga}}$ (cm^2/s)	Initial $[V_{Ga}]$ in SL (cm^{-3})	Initial $[V_{Ga}]$ in substrate (cm^{-3})	GoF
SnA	Sn	Erf	1000	$7.0 \pm 0.5 \times 10^{-31}$	$6 \pm 1 \times 10^{-14}$	0	10^{16}	0.011 85
SnA	Sn	Linear	1000	$6.0 \pm 0.5 \times 10^{-31}$	$4 \pm 1 \times 10^{-13}$	0	10^{16}	0.014 11
SnB	Sn	Erf	1050	$2.7 \pm 0.1 \times 10^{-30}$	$6 \pm 1 \times 10^{-14}$	0	10^{16}	0.009 56
SnB	Sn	Linear	1050	$2.7 \pm 0.2 \times 10^{-30}$	$4 \pm 0.3 \times 10^{-13}$	0	10^{16}	0.005 28
SnC	Sn	Erf	1100	$8.0 \pm 1.0 \times 10^{-30}$	$4 \pm 1 \times 10^{-14}$	2.0×10^{13}	2×10^{15}	0.012 44
SnC	Sn	Linear	1100	$8.0 \pm 1.0 \times 10^{-30}$	$1.3 \pm 0.2 \times 10^{-12}$	0	2×10^{15}	0.019 11
Fe	Fe	NA	1050	$3.5 \pm 0.5 \times 10^{-32}$	N/A	0	10^{16}	0.051 88
E_A (eV)				3.9 ± 0.3	2.0 ± 1.2			

diffusion scales with $[V_{Ga}]$, the details of the leading edge will not dominate the time-integrated Al diffusion. The difference between the classical *erf*() solution and piecewise linear R–D profiles may be seen by comparing the green dashed curves in Figs. 2(d) and 2(e). Figure 2(e) shows fitting of one example dataset using the piecewise linear model for the evolution of $[V_{Ga}](x,t)$. By inspection, the Al diffusion is also well-described using this model for V_{Ga} diffusion and Table I shows that statistically similar GoF values are obtained for both models.

The best-fit model for Al diffusion assuming *erf*() diffusion for $[V_{Ga}]$ suggests that a significant gradient of $[V_{Ga}]$ (and thus Sn_{Ga}) should remain at the end of our experiments, while the RD model and our piecewise approximation thereof predict that $[V_{Ga}]$ and [Sn] should be closer to uniform at the end of the experiment. The latter is in agreement with the measured, nearly uniform final [Sn] profiles as exemplified by Fig. 1(b). In addition, using the piecewise linear approximation allows us to recover the Arrhenius behavior for both Al and V_{Ga}. Moreover, the $D_{V_{Ga}}$ values extracted using the piecewise linear model smoothly join with those from Ref. 24 despite $D_{V_{Ga}}$ being extracted from our [Al] profiles and from [Sn] profiles in theirs, indicating that in both cases the diffusivity of Sn_{Ga}–V_{Ga} complexes or at least the interactions between Sn_{Ga} and V_{Ga} determine the rate limiting step(s). We take these observations as confirmations that the piecewise R–D approximation for V_{Ga} diffusion more accurately represents the microscopics of V_{Ga} diffusion in these SLs.

A subtle point is that our modeling using either the *erf*() or piecewise linear models explains the Al diffusion assuming that V_{Ga} originate in the substrate and that their total number is conserved at least to a tolerance of a few percent. However, in Ref. 24, V_{Ga} were assumed to appear via unspecified generation or transport processes as needed to maintain local equilibrium with the diffusing Sn—in other words that V_{Ga} may not be conserved. The supplementary material contains a thorough discussion of this issue as far as it can be addressed in the current work. Succinctly, the lower extent of diffusion of Al close to the free surface rules out large concentrations of $[V_{Ga}]$ being injected there ("large" relative to at. % concentrations of Al). Since the concentrations of Sn in Ref. 24 range from 10^{14} to 10^{18}/cm^3, these experiments are sensitive to much lower concentrations of V_{Ga}. The high-concentration features of the [Sn](x,t) R–D diffusion front shape can be reproduced assuming that V_{Ga} is conserved; however, the low-concentration leading tail cannot be reproduced. Thus, we can only conclude that any bulk generation or injection of V_{Ga} must be below the capability of the present experiments to resolve. Resolution of these fine details should be possible in future experiments using smaller tracer concentrations designed to identify and quantify the mechanisms introducing V_{Ga} during annealing under oxidizing conditions. The lack of evidence for $[V_{Ga}]$ in-diffusion from the free surface in our [Al] data herein raises a question for future investigations: what sources, sinks, and transport processes for $[V_{Ga}]$ operate in order to establish equilibration with local Fermi levels and p_{O_2} during annealing and growth? However, for the immediate purpose of analyzing our Al diffusion data, this question is immaterial since the R–D models predict the free $[V_{Ga}]$ able to facilitate Al diffusion to have functional shape closely mimicking the Sn profile.

The sample annealed at 1050 °C [Fig. 2(b)] exhibits a greater extent of diffusion than the one annealed at 1100 °C [Fig. 2(c)], counter to what would be expected for Arrhenius activation if the two samples had identical initial concentrations of $[V_{Ga}]$. This was initially a source of great consternation until we realized that the sample annealed at 1100 °C [Fig. 2(c)] was grown in an earlier growth run using a different substrate, while the samples annealed at 1000 and 1050 °C [Figs. 2(a) and 2(b)] were grown at a later date on pieces of a different Sn-doped (010) $\beta - Ga_2O_3$ wafer. $[V_{Ga}]$ is likely to vary spatially even within the same EFG-grown bulk crystal; thus, some variation from wafer to wafer should not be surprising. Likewise, despite using nominally the same growth recipe for all three samples, some variation is reasonably likely in $[V_{Ga}]$ within the SL between growth runs.

The finite difference model in Sec. II ultimately depends on $D_{Al}(x,t)$ as defined in Eq. (1); thus, fitting via simulation does not directly measure $[V_{Ga}]$ but rather the $D_{oo}(T) \times [V_{Ga}](x,t)$ product. In our final analysis, we conclude that $[V_{Ga}] = 10^{16}$/cm^3 in the substrates for the 1000 and 1050 °C annealed samples, but explored possibilities that the substrate and SL for the 1100 °C sample had different $[V_{Ga}]$. In all cases, the value of $[V_{Ga}]$ in the SL was determined independently for each sample through the fitting process. After testing a wide range of scenarios, the data from the 1100 °C

sample are best explained by lower initial $[V_{Ga}] = 2 \times 10^{15}/cm^3$ in that sample's substrate. A more sensible behavior for $D_{oo}(T)$ compatible with an Arrhenius law with activation energy 3.9 ± 0.3 eV is obtained, which is comparable to the value of 4.2 eV obtained for Al_{Ga} diffusion in (−201) $\beta - Ga_2O_3$ in Ref. 49. Table I summarizes the final best-fit parameters for both $erf()$ and piecewise linear models for V_{Ga} diffusion, and Fig. 4 shows our data in the context of the existing literature.

In Figs. 1(a) and 1(b), we compare two SLs annealed at 1050 °C on Fe- and Sn-doped substrates. On the Sn-doped substrate, the best-fit scenario within the piecewise linear model of V_{Ga} diffusion yields $D_{oo} = 2.7 \times 10^{-30}$ cm^5/s at an initial value of $[V_{Ga}] = 10^{16}/cm^3$ in the substrate. D_{oo} for Al in the absence of V_{Ga} complexing with Sn would be expected to be the same or larger, depending on how significantly the presence of Sn limits the ability of V_{Ga} to mediate Al diffusion. If we do assume that D_{oo} is the same for samples grown on both Fe- and Sn-doped substrates, we estimate that the initial $[V_{Ga}]$ in the substrate for samples grown on Fe-doped substrates would be $10^{14}/cm^3$, or ≈100 times lower that for the Sn-doped substrates. This is on the lower end of the range of estimated ratios based on expected Fermi level positions, but given the lack of direct comparison data and uncertainty regarding the effects of Sn and Fe co-diffusing with V_{Ga}, considered reasonable.

VI. DIFFUSION OF UNINTENTIONAL IMPURITIES

In addition to the d-SIMS of Al, Fe, and Sn presented so far, we also used ToF-SIMS 3D reconstructions and survey d-SIMS detecting all elements present (at lower spatial and concentration resolutions than Al profiles). These revealed that many other elements besides Fe or Sn also diffuse out of Sn-doped substrates, through the SLs, and accumulated at the free surfaces. Figure 3 shows the concentration-calibrated SIMS profiles for five illustrative metals present in the SL shown in Fig. 2(b), annealed at 1000 °C. After collecting the 20 h annealed SIMS profile shown in Fig. 2(b), the sample was immersed in aqua regia for 10 min to remove any possibility of metal contamination at the surface and then annealed in O_2 for an additional 10 h (total 30 h) as part of efforts to eliminate the possibility of Fe surface contamination diffusing into the SL while annealing inside the tube furnace (supplementary material). Given the known presence of many of these elements in wafers grown from melts held in Ir crucibles—e.g., EFG[43,47] and the high purity of OMVPE-grown layers, we infer that these elements diffused into the SLs from the substrate.

Mn, Fe, and Ni accumulate at the surface to depths that are incompatible with typical SIMS artifacts. [Cu] exhibits a concentration peak around the middle of the SL, perhaps indicating interactions between its charge states and the Fermi level within a space charge region. All these transition metals are likely capable of multiple interstitial and substitutional diffusion modes in multiple charge states. Ti was also detected at $10^{16}/cm^3$ uniform in depth through the d-SIMS survey scan, while Si and Na were also detected in ToF-SIMS. Li being extremely small is suspected to be capable of fast interstitial diffusion and is depleted rather than enriched close to the surface. These different behaviors are consistent with an electrochemical potential gradient affecting different elements and charge states differently near the surface. A depletion width and built-in potential $\phi(x)$ induced by surface Fermi level pinning is the simplest example, and defects with different relative charges q would accumulate or deplete as $\exp\left(\frac{q\phi(x)}{k_B T}\right)$ self-consistently following the Poisson–Boltzmann equation. However, it has been frequently observed that $\beta - Ga_2O_3$ surfaces, especially in the presence of additional impurities, can change to the different $\gamma - Ga_2O_3$ phase, which would of course change the chemical potential for each impurity, perhaps causing them to accumulate. Further analysis of these profiles is beyond the scope of this work, but the observation of these impurities, some like Cu, Na, and Li being notoriously fast diffusers in semiconductors, calls for further quantification of impurities and their diffusion in multiple phases of Ga_2O_3 and in devices from fabrication to long-term degradation under high fields and temperatures.

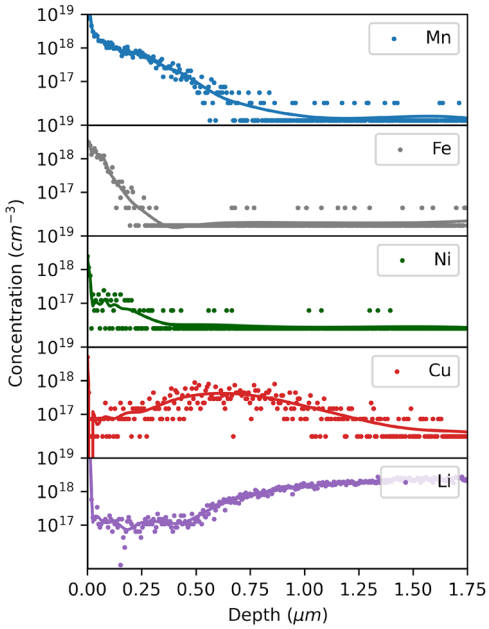

FIG. 3. Low spatial and concentration resolution "survey" SIMS profiles of five species, which show a high concentration and non-homogenous behavior for the SL on the Sn-doped substrate annealed at 1000 °C for 30 h in oxygen. Each survey is fit with a univariate spline function (solid line).

VII. CONTEXTUALIZING RESULTS

Figure 4 compares the measured and computed diffusivities in Ga_2O_3 from this work and that from the literature. Our values of $D_{V_{Ga}}$ extracted using the piecewise linear model for R–D have remarkable agreement with the diffusion of Sn_{Ga}–V_{Ga} complexes reported by Frodason[24] and follow a sensible Arrhenius trend with activation energy 1.96 ± 1.19 eV. Our values extracted with the $erf(x,t)$ model are an order of magnitude lower and deviate from the Arrhenius behavior. The blue rhombuses plot the free diffusion of uncomplexed V_{Ga} from Ref. 24 and are at least three orders of magnitude faster than our results for the vacancies responsible for Al diffusion under either scenario, which is consistent with our conclusion that the co-diffusing Sn also slows the progress of V_{Ga} in our experiments.

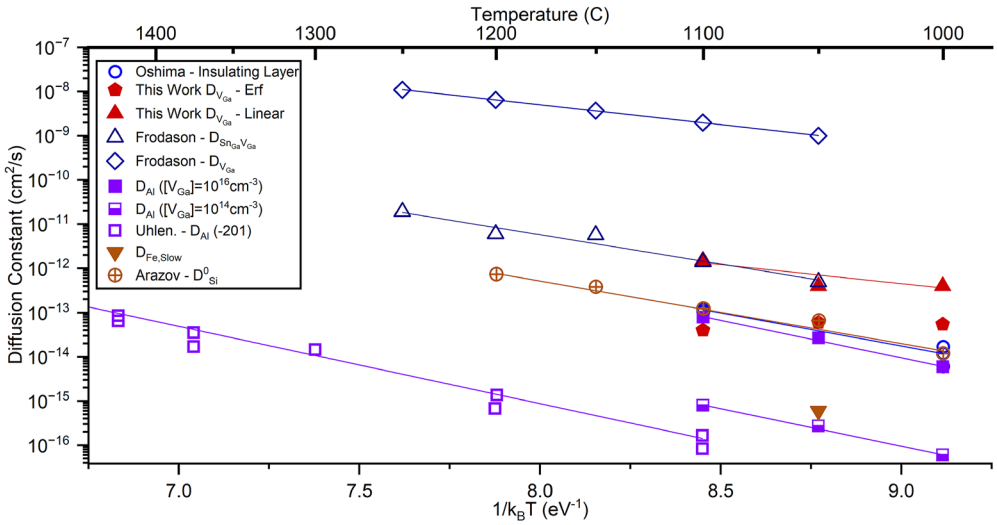

FIG. 4. Arrhenius plot of data in the present work along with data from the existing literature. Our values of $D_{V_{Ga}}$ extracted using the *erf*( ) and piecewise linear models are shown as red pentagons and triangles, respectively. The diffusion constants required for insulating layers measured in Ref. 5 are shown as blue circles. $D_{V_{Ga}}$ and $D_{Sn_{Ga}-V_{Ga}}$ from Ref. 24 are shown as blue rhombuses and triangles, respectively. Based on our extracted values of $D_{oo}(T)$ for Al, we present D_{Al} for two concentrations of V_{Ga} [see Eq. (1)]: $[V_{Ga}] = 10^{16}$ cm^{-3} appropriate for Al in Sn-doped wafers (purple solid squares) and $[VG_{Ga}] = 10^{14}$ cm^{-3} appropriate for semi-insulating or oxygen annealed samples (half-filled purple squares). The latter agrees well with recently published data by Uhlendorf and Schmitt.[49] D_{Fe} extracted from the slow-diffusing component in Fig. 1(a) is shown as inverted brown triangles. In addition, D^0_{Si} from Ref. 50 is shown as brown crossed-circles; this follows a similar activation energy but is apparently slightly slower than the diffusion of (Sn_{Ga}–V_{Ga}) complexes.

Since $D_{oo,Al}(T)$ cannot be shown directly on this plot, we multiply it by two different $[V_{Ga}]$ to show the range of D_{Al} expected in most situations aside from, for example, ion implantation. $[V_{Ga}] = 10^{16}/cm^3$ represents equilibrated conditions for heavy *n*-type doping as in Sn-doped EFG-grown wafers, while $[V_{Ga}] = 10^{14}/cm^3$ may be expected in UID to insulating conditions as found for our SLs on Fe-doped substrates. This latter set is in good agreement with D_{Al} derived from the interdiffusion of a thin Al_2O_3 layer on Ga_2O_3 during oxygen annealing.[49]

The inverted brown triangles show D_{Fe} for the slow diffusion channel from Fe-doped substrates into the SLs. This value is similar to those experienced by Al, so we speculate that it may be vacancy-mediated but modified by the expected Coulomb repulsion between V_{Ga} and Fe_{Ga} acceptors compared to the case of Al. Further detailed studies will be needed to understand the diffusion of Fe and other metals prone to charge state changes and possibly diffusing by multiple mechanisms simultaneously.

Oshima *et al.* used capacitance methods to measure the expansion of an insulating layer on the surface of *n*-type samples up to a few μm thickness during O_2 annealing. The kinetics of layer thickening were consistent with a diffusion-limited process; thus, we plot their diffusion constants derived from thickness = $\sqrt{Dt}$ as blue circles. These diffusion constants are consistent with the vacancy-mediated diffusion of Sn, Si, and Al under *n*-type conditions found herein and in Refs. 49 and 24. As discussed in Sec. VI, the conversion of surface layers to insulating may also include surface band bending and possibly phase changes to γ-Ga_2O_3. Clearly, there are many questions to be explored with direct experiment and theory in the diffusion and annealing behavior of native defects and impurities in Ga_2O_3.

VIII. CONCLUSIONS

In this work, we investigated the diffusion of V_{Ga} using specially designed superlattices that allow gradients in the extent of diffusion and thus history of $[V_{Ga}]$ to be inferred. V_{Ga} are available in great numbers in Sn-doped substrates, transiently diffusing outward toward the epilayers in our experiments. This allowed us to measure D_{VGa}, which we found was significantly affected by its co-diffusion with Sn donors. We developed a novel finite difference scheme, in which the diffusion of impurities such as Al is dependent on the local concentration of V_{Ga}. We find no evidence for Ga vacancies introduced from the surface significantly affecting the Al diffusion, although these may be introduced at lower concentrations. The diffusion rates extracted for V_{Ga} are far lower than those predicted for free vacancies based on DFT calculations. Instead, they are retarded by the strong Coulomb attraction to donors such as Sn and Si highlighting that that doping will have indirect effects on Ga self-diffusion and on isovalent Al diffusion. Diffusion and surface accumulation of unintentionally introduced impurities such as Fe, Mn, Cu, and Li bear further exploration, including the effects of surface potential and phase changes.

SUPPLEMENTARY MATERIAL

See the supplementary material for the derivation of the piecewise linear approximation of the reaction diffusion of Sn_{Ga}–V_{Ga} complexes and quantitative comparison with the numerical solutions described in Ref. 24. The supplementary material also contains a discussion reconciling an apparent contradiction in *a priori* assumptions on the conservation or non-conservation of V_{Ga} in our

modeling and that described in Ref. 24, and an analysis of the effects of lateral non-uniformity in d-SIMS profiles. It also describes our efforts to validate the apparent accumulation of Fe at the surface during annealing and eliminate the possibility that this is either a SIMS artifact or a result of surface contamination.

ACKNOWLEDGMENTS

This work was funded by the Air Force Office of Scientific Research—Multidisciplinary Research Program of the University Research Initiative (MURI)—AFOSR under Award Nos. FA9550-18-1-0507 and FA9550-21-0078. We also thank Northrop Grumman-Synoptics and John Blevins for $\beta - Ga_2O_3$ boule pieces. We thank K. M. Johansen and Y. K. Frodason for the use of their data and modeling of Sn_{Ga} and V_{Ga} reaction–diffusion. We thank D. Feezell and his group for high-resolution x-ray diffraction scans on early samples to help characterize the growth rate variations and F. Guervara-Vasquez for informative discussions on finite difference schemes.

AUTHOR DECLARATIONS

Conflict of Interest

The authors have no conflicts to disclose.

Author Contributions

Nathan D. Rock: Conceptualization (equal); Data curation (equal); Formal analysis (equal); Investigation (equal); Methodology (equal); Resources (equal); Writing – original draft (equal); Writing – review & editing (equal). **Haobo Yang**: Conceptualization (equal); Data curation (supporting); Formal analysis (supporting); Funding acquisition (equal); Investigation (supporting); Methodology (equal); Project administration (equal); Resources (equal); Supervision (equal); Writing – review & editing (equal). **Brian Eisner**: Data curation (supporting); Investigation (supporting). **Aviva Levin**: Data curation (supporting); Investigation (supporting). **Arkka Bhattacharyya**: Formal analysis (supporting); Resources (supporting). **Sriram Krishnamoorthy**: Data curation (supporting); Investigation (supporting); Resources (supporting). **Praneeth Ranga**: Resources (supporting). **Michael A Walker**: Conceptualization (equal); Formal analysis (supporting); Funding acquisition (equal); Investigation (equal); Methodology (equal); Project administration (equal); Resources (equal); Supervision (equal); Writing – review & editing (equal). **Larry Wang**: Data curation (supporting). **Ming Kit Cheng**: Data curation (supporting). **Wei Zhao**: Data curation (supporting); Investigation (supporting). **Michael A. Scarpulla**: Conceptualization (equal); Data curation (equal); Formal analysis (equal); Funding acquisition (equal); Investigation (equal); Methodology (equal); Project administration (equal); Resources (equal); Supervision (equal); Writing – original draft (equal); Writing – review & editing (equal).

DATA AVAILABILITY

The data that support the findings of this study are available within the article and its supplementary material.

REFERENCES

[1] S. J. Pearton, J. Yang, P. H. Cary, F. Ren, J. Kim, M. J. Tadjer, and M. A. Mastro, "A review of Ga_2O_3 materials, processing, and devices," Appl. Phys. Rev. **5**, 011301 (2018).

[2] A. J. Green, J. Speck, G. Xing, P. Moens, F. Allerstam, K. Gumaelius, T. Neyer, A. Arias-Purdue, V. Mehrotra, A. Kuramata, K. Sasaki, S. Watanabe, K. Koshi, J. Blevins, O. Bierwagen, S. Krishnamoorthy, K. Leedy, A. R. Arehart, A. T. Neal, S. Mou, S. A. Ringel, A. Kumar, A. Sharma, K. Ghosh, U. Singisetti, W. Li, K. Chabak, K. Liddy, A. Islam, S. Rajan, S. Graham, S. Choi, Z. Cheng, and M. Higashiwaki, "β-Gallium oxide power electronics," APL Mater. **10**, 029201 (2022).

[3] J. Y. Tsao, S. Chowdhury, M. A. Hollis, D. Jena, N. M. Johnson, K. A. Jones, R. J. Kaplar, S. Rajan, C. G. Van de Walle, E. Bellotti, C. L. Chua, R. Collazo, M. E. Coltrin, J. A. Cooper, K. R. Evans, S. Graham, T. A. Grotjohn, E. R. Heller, M. Higashiwaki, M. S. Islam, P. W. Juodawlkis, M. A. Khan, A. D. Koehler, J. H. Leach, U. K. Mishra, R. J. Nemanich, R. C. N. Pilawa-Podgurski, J. B. Shealy, Z. Sitar, M. J. Tadjer, A. F. Witulski, M. Wraback, and J. A. Simmons, "Ultrawide-bandgap semiconductors: Research opportunities and challenges," Adv. Electron. Mater. **4**, 1600501 (2018).

[4] T. Oshima, T. Okuno, N. Arai, N. Suzuki, S. Ohira, and S. Fujita, "Vertical solar-blind deep-ultraviolet Schottky photodetectors based on β-Ga_2O_3 substrates," Appl. Phys. Express **1**, 011202 (2008).

[5] T. Oshima, K. Kaminaga, A. Mukai, K. Sasaki, T. Masui, A. Kuramata, S. Yamakoshi, S. Fujita, and A. Ohtomo, "Formation of semi-insulating layers on semiconducting β-Ga_2O_3 single crystals by thermal oxidation," Jpn. J. Appl. Phys. **52**, 051101 (2013).

[6] Y.-J. Lee, M. A. Schweitz, J.-M. Oh, and S.-M. Koo, "Influence of annealing atmosphere on the characteristics of Ga_2O_3/4H-SiC n-n heterojunction diodes," Materials **13**, 434 (2020).

[7] J. B. Varley, J. R. Weber, A. Janotti, and C. G. Van de Walle, "Oxygen vacancies and donor impurities in β-Ga_2O_3," Appl. Phys. Lett. **97**, 142106 (2010).

[8] F. Tuomisto and I. Makkonen, "Defect identification in semiconductors with positron annihilation: Experiment and theory," Rev. Mod. Phys. **85**, 1583–1631 (2013).

[9] E. Korhonen, F. Tuomisto, D. Gogova, G. Wagner, M. Baldini, Z. Galazka, R. Schewski, and M. Albrecht, "Electrical compensation by Ga vacancies in Ga_2O_3 thin films," Appl. Phys. Lett. **106**, 242103 (2015).

[10] M. E. Ingebrigtsen, A. Yu. Kuznetsov, B. G. Svensson, G. Alfieri, A. Mihaila, U. Badstübner, A. Perron, L. Vines, and J. B. Varley, "Impact of proton irradiation on conductivity and deep level defects in β-Ga_2O_3," APL Mater. **7**, 022510 (2019).

[11] J. Jesenovec, M. H. Weber, C. Pansegrau, M. D. McCluskey, K. G. Lynn, and J. S. McCloy, "Gallium vacancy formation in oxygen annealed β-Ga_2O_3," J. Appl. Phys. **129**, 245701 (2021).

[12] Y. K. Frodason, C. Zimmermann, E. F. Verhoeven, P. M. Weiser, L. Vines, and J. B. Varley, "Multistability of isolated and hydrogenated Ga–O divacancies in β-Ga_2O_3," Phys. Rev. Mater. **5**, 025402 (2021).

[13] A. Karjalainen, P. M. Weiser, I. Makkonen, V. M. Reinertsen, L. Vines, and F. Tuomisto, "Interplay of vacancies, hydrogen, and electrical compensation in irradiated and annealed n-type β-Ga_2O_3," J. Appl. Phys. **129**, 165702 (2021).

[14] A. Kyrtsos, M. Matsubara, and E. Bellotti, "Migration mechanisms and diffusion barriers of vacancies in Ga_2O_3," Phys. Rev. B **95**, 245202 (2017).

[15] R. Sun, Y. K. Ooi, P. Ranga, A. Bhattacharyya, S. Krishnamoorthy, and M. A. Scarpulla, "Oxygen annealing induced changes in defects within β-Ga_2O_3 epitaxial films measured using photoluminescence," J. Phys. D: Appl. Phys. **54**, 174004 (2021).

[16] R. A. De Souza and J. A. Kilner, "Oxygen transport in $La_{1-x}Sr_xMn_{1-y}Co_yO_{3\pm\delta}$ perovskites: Part I. Oxygen tracer diffusion," Solid State Ionics **106**, 175–187 (1998).

[17] J. Töpfer, S. Aggarwal, and R. Dieckmann, "Point defects and cation tracer diffusion in $(Cr_xFe_{1-x})_{3-\delta}O_4$ spinels," Solid State Ionics **81**, 251–266 (1995).

[18] R. E. Howard, "Random-walk method for calculating correlation factors: Tracer diffusion by divacancy and impurity-vacancy pairs in cubic crystals," Phys. Rev. **144**, 650–661 (1966).

[19] P. Klugkist and C. Herzig, "Tracer diffusion of titanium in α-iron," Phys. Status Solidi A **148**, 413–421 (1995).

[20]H. Mehrer, *Diffusion in Solids: Fundamentals, Methods, Materials, Diffusion-Controlled Processes* (Springer Science & Business Media, 2007).
[21]S. T. Dunham and C. D. Wu, "Atomistic models of vacancy-mediated diffusion in silicon," J. Appl. Phys. **78**, 2362–2366 (1995).
[22]E. G. Seebauer and M. C. Kratzer, "Charged semiconductor defects: Structure, thermodynamics and diffusion," in *Engineering Materials and Processes* (Springer, London, 2009).
[23]K. M. Johansen, L. Vines, T. S. Bjørheim, R. Schifano, and B. G. Svensson, "Aluminum migration and intrinsic defect interaction in single-crystal zinc oxide," Phys. Rev. Appl. **3**, 024003 (2015).
[24]Y. K. Frodason, P. P. Krzyzaniak, L. Vines, J. B. Varley, C. G. Van de Walle, and K. M. H. Johansen, "Diffusion of Sn donors in β-Ga_2O_3," APL Mater. **11**, 041121 (2023).
[25]H. Bracht, "Diffusion mechanisms and intrinsic point-defect properties in silicon," MRS Bull. **25**, 22–27 (2000).
[26]U. M. Gösele and T. Y. Tan, "Point defects and diffusion in semiconductors," MRS Bull. **16**, 42–46 (1991).
[27]P. Pichler, in *Intrinsic Point Defects, Impurities, and Their Diffusion in Silicon*, edited by S. Selberherr and C. Microelectronics (Springer, Vienna, 2004).
[28]R. Vaidyanathan, M. Y. L. Jung, R. D. Braatz, and E. G. Seebauer, "Measurement of defect-mediated diffusion: The case of silicon self-diffusion," AIChE J. **52**, 366–370 (2006).
[29]P. M. Fahey, P. B. Griffin, and J. D. Plummer, "Point defects and dopant diffusion in silicon," Rev. Mod. Phys. **61**, 289–384 (1989).
[30]M. J. Tadjer, C. Fares, N. A. Mahadik, J. A. Freitas, D. Smith, R. Sharma, M. E. Law, F. Ren, S. J. Pearton, and A. Kuramata, "Damage recovery and dopant diffusion in Si and Sn ion implanted β-Ga_2O_3," ECS J. Solid State Sci. Technol. **8**, Q3133 (2019).
[31]A. Nikolskaya, E. Okulich, D. Korolev, A. Stepanov, D. Nikolichev, A. Mikhaylov, D. Tetelbaum, A. Almaev, C. A. Bolzan, A. Buaczik, Jr., R. Giulian, P. L. Grande, A. Kumar, M. Kumar, and D. Gogova, "Ion implantation in β-Ga_2O_3: Physics and technology," J. Vac. Sci. Technol., A **39**, 030802 (2021).
[32]S. T. Dunham and J. D. Plummer, "Point-defect generation during oxidation of silicon in dry oxygen. I. Theory," J. Appl. Phys. **59**, 2541–2550 (1986).
[33]B. Hobbs and A. Ord, "Chapter 9—Visco-plastic flow," in *Structural Geology*, edited by B. Hobbs and A. Ord (Elsevier, Oxford, 2015), pp. 287–326.
[34]D. Krasikov and I. Sankin, "Beyond thermodynamic defect models: A kinetic simulation of arsenic activation in CdTe," Phys. Rev. Mater. **2**, 103803 (2018).
[35]*MATLAB version: 9.13.0 (R2022b)*, The MathWorks, Inc., 2022.
[36]K. Jacobs, "F. A. Kröger. The Chemistry of Imperfect Crystals. 2nd Revised Edition, Volume 1: Preparation, Purification, Crystal Growth And Phase Theory. North-Holland Publishing Company—Amsterdam/London 1973 American Elsevier Publishing Company, Inc.—New York 313 Seiten, zahlreiche Abbildungen und Tabellen, Kunstleder Preis Dfl. 70.00," Krist. Tech. **9**, K67–K68 (1974).
[37]J. B. Varley, "First-principles calculations 2," in *Gallium Oxide: Materials Properties, Crystal Growth, and Devices*, *Springer Series in Materials Science*, edited by M. Higashiwaki and S. Fujita (Springer International Publishing, Cham, 2020), pp. 329–348.
[38]H. J. von Bardeleben, G. He, Y. Wu, and S. Ding, "High temperature annealing of n-type bulk β-Ga_2O_3: Electrical compensation and defect analysis—The role of gallium vacancies," J. Appl. Phys. **134**, 165702 (2023).
[39]F. Tuomisto, "Identification of point defects in multielement compounds and alloys with positron annihilation spectroscopy: Challenges and opportunities," Phys. Status Solidi RRL **15**, 2100177 (2021).
[40]H. Ghadi, J. F. McGlone, C. M. Jackson, E. Farzana, Z. Feng, A. F. M. A. U. Bhuiyan, H. Zhao, A. R. Arehart, and S. A. Ringel, "Full bandgap defect state characterization of β-Ga_2O_3 grown by metal organic chemical vapor deposition," APL Mater. **8**, 021111 (2020).
[41]J. M. Johnson, Z. Chen, J. B. Varley, C. M. Jackson, E. Farzana, Z. Zhang, A. R. Arehart, H.-L. Huang, A. Genc, S. A. Ringel, C. G. Van de Walle, D. A. Muller, and J. Hwang, "Unusual Formation of point-defect complexes in the ultrawide-band-gap semiconductor β-Ga_2O_3," Phys. Rev. X **9**, 041027 (2019).
[42]Z. Galazka, R. Uecker, K. Irmscher, M. Albrecht, D. Klimm, M. Pietsch, M. Brützam, R. Bertram, S. Ganschow, and R. Fornari, "Czochralski growth and characterization of β-Ga_2O_3 single crystals," Cryst. Res. Technol. **45**, 1229–1236 (2010).
[43]A. Kuramata, K. Koshi, S. Watanabe, Y. Yamaoka, T. Masui, and S. Yamakoshi, "High-quality β-Ga_2O_3 single crystals grown by edge-defined film-fed growth," Jpn. J. Appl. Phys. **55**, 1202A2 (2016).
[44]Z. Zhang, E. Farzana, A. R. Arehart, and S. A. Ringel, "Deep level defects throughout the bandgap of (010) β-Ga_2O_3 detected by optically and thermally stimulated defect spectroscopy," Appl. Phys. Lett. **108**, 052105 (2016).
[45]M. E. Ingebrigtsen, J. B. Varley, A. Yu. Kuznetsov, B. G. Svensson, G. Alfieri, A. Mihaila, U. Badstübner, and L. Vines, "Iron and intrinsic deep level states in Ga_2O_3," Appl. Phys. Lett. **112**, 042104 (2018).
[46]J. Crank, The mathematics of diffusion (1956).
[47]J. S. McCloy, J. Jesenovec, B. L. Dutton, C. Pansegrau, C. Remple, M. H. Weber, S. Swain, M. McCluskey, M. Scarpulla, J. S. McCloy, J. Jesenovec, B. L. Dutton, C. Pansegrau, C. Remple, M. H. Weber, S. Swain, M. McCluskey, and M. Scarpulla, "Growth and defect characterization of doped and undoped β-Ga_2O_3 crystals," Proc. SPIE **12002**, 1200205 (2022).
[48]S. T. Dunham, "A quantitative model for the coupled diffusion of phosphorus and point defects in silicon," J. Electrochem. Soc. **139**, 2628 (1992).
[49]J. Uhlendorf and H. Schmidt, "Oxygen and aluminum tracer diffusion in (−201) oriented β-Ga_2O_3 single crystals," Phys. Rev. Mater. **7**, 093402 (2023).
[50]A. Azarov, V. Venkatachalapathy, L. Vines, E. Monakhov, I.-H. Lee, and A. Kuznetsov, "Activation energy of silicon diffusion in gallium oxide: Roles of the mediating defects charge states and phase modification," Appl. Phys. Lett. **119**, 182103 (2021).